JACS
JOURNAL OF THE AMERICAN CHEMICAL SOCIETY
Cite This: J. Am. Chem. Soc. 2019, 141, 12989−12993
Communication
pubs.acs.org/JACS

Dynamic Electric Field Alignment of Metal−Organic Framework Microrods

Fei Cheng,[†,¶] Adam J. Young,[†,‡,¶] Jean-Sebastien G. Bouillard,[§] Neil T. Kemp,[§] Rémy Guillet-Nicolas,[∥] Connor H. Hall,[§] David Roberts,[†] Ayoub H. Jaafar,[§] Ali M. Adawi,[§] Freddy Kleitz,[∥] Arnout Imhof,[⊥] Michael R. Reithofer,*[,‡] and Jia Min Chin*[,†,‡]

[†]Department of Chemistry, University of Hull, Hull HU6 7RX, United Kingdom
[‡]Institute of Inorganic Chemistry, Faculty of Chemistry, University of Vienna, Vienna A-1090, Austria
[§]Department of Physics and Mathematics, University of Hull, Hull HU6 7RX, United Kingdom
[∥]Department of Inorganic Chemistry - Functional Materials, Faculty of Chemistry, University of Vienna, Vienna A-1090, Austria
[⊥]Soft Condensed Matter & Biophysics, Debye Institute for Nanomaterials Science, Utrecht University, Utrecht 3584 CC, The Netherlands

Supporting Information

ABSTRACT: Alignment of metal−organic framework (MOF) crystals has previously been performed via careful control of oriented MOF growth on substrates, as well as by dynamic magnetic alignment. We show here that bromobenzene-suspended microrod crystals of the MOF NU-1000 can also be dynamically aligned via electric fields, giving rise to rapid electrooptical responses. This method of dynamic MOF alignment opens up new avenues of MOF control which are important for integration of MOFs into switchable electronic devices as well as in other applications such as reconfigurable sensors or optical systems.

Metal−organic frameworks (MOFs), which are crystalline materials composed of inorganic nodes linked by organic ligands, are of significant research interest due to their flexible choice of linkers and metals which afford them wide-ranging applications[1−3] such as in optics, sensing, electronics, gas separations and energy storage.

When considering MOFs for applications, it should be noted that as most MOFs possess lattice anisotropy along different crystallographic axes, their corresponding physicochemical properties also significantly differ along different crystallographic directions. Therefore, to fully exploit directional functionality of MOFs, it is important to control MOF particle orientation. However, as MOF materials are typically synthesized as loose colloidal powders, it is challenging to impose and integrate particle orientational control into their utilization. Research has consequently focused on growth of MOF crystals on various substrates, to favor selective directional growth.[4−6] Unfortunately, this is time-consuming, and significant care must be taken to control crystal growth. Furthermore, the growth conditions for one type of MOF cannot simply be applied wholesale to other MOFs, with considerations of MOF-substrate lattice matching and interfacial physicochemical interactions complicating the widespread application of this approach.[7] Significantly, this approach renders the MOF orientation static, hindering the use of MOFs in applications requiring dynamicity, such as in stimuli-responsive devices, whereby the MOFs can reorient themselves under changing conditions. Given the vast applicability of MOFs, dynamic control of MOF alignment will have significant implications for many areas.

The long-range molecular order imposed by the MOF lattices, and their tunable physicochemical properties, also render MOFs especially attractive for use in electronic devices.[8] E-field control of MOFs is therefore particularly desirable, and there are emerging reports of external E-field MOF manipulation. Examples include current driven synthesis of ZIF-8,[9] field-driven rotation of MOF ligands,[10,11] as well as the E-field induced polymorph switching of ZIF-8[12] and MIL-53.[13−15] Reports pertaining to control of MOF crystal assembly include their electrophoretic deposition into electroactive thin films,[1016] and the assembly of polyhedral ZIF-8 microparticles into locked chains under an alternating E-field,[17] whereby the flat particle facets allowed for interparticle facet-to-facet adhesion through van der Waals forces, as the alternating E-field polarized the electrostatic double layer. Further, Choi et al. showed that suspensions of $Cu_3(BTC)_2$ in silicone oil possessed electrorheological properties, whereby E-field application leads to $Cu_3(BTC)_2$ particle chaining.[18] Nevertheless, reports of E-field control of MOF particle assembly are still extremely sparse, and have not focused on switchable control of MOF orientation despite the promise this area offers.

NU-1000, a zirconium-based MOF, possesses an anisotropic lattice, composed of 8-connected $Zr_6(\mu_3\text{-}OH)_4(\mu_3\text{-}O)_4(OH)_4(OH_2)_4$ nodes linked by tetratopic 1,3,6,8-tetrakis-(*p*-benzoate)pyrene (TBAPy) ligands.[19,20] 31 Å hexagonal channels and 12 Å triangular channels are oriented along the *c*-axis of NU-1000 crystals (Figure 1) and smaller 10 Å pores perpendicular to these channels, resulting in anisotropic molecular diffusivity[21] and photophysical properties for NU-1000.[22]

Received: June 13, 2019
Published: August 5, 2019

DOI: 10.1021/jacs.9b06320
J. Am. Chem. Soc. 2019, 141, 12989−12993

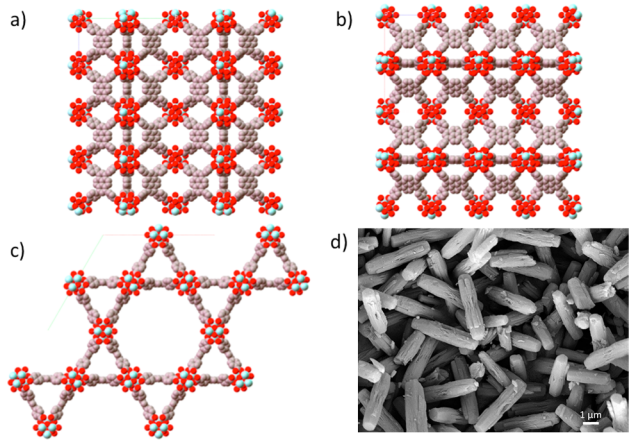

Figure 1. (a–c) View of NU-1000 lattice along the *a*, *b* and *c* crystallographic axes respectively, showing the lattice anisotropy. (d) Scanning electron micrograph of NU-1000 microrods showing shape anisotropy of the particles.

We previously showed that magnetized NU-1000 could be dynamically aligned via magnetic fields.[22] However, the use of E-fields for MOF alignment would significantly widen the scope for device integration as it is simpler and more practical to implement for many applications. E-fields also have a greater dynamic range of field strengths and are easier to localize, avoiding cross-talk or interference within devices. Here we demonstrate, for the first time, the utilization of E-fields to dynamically and reversibly control NU-1000 alignment. NU-1000 was selected for these investigations, due to its lattice and particle shape anisotropy, high chemical and thermal stability, large specific surface area, synthetic scalability,[23] as well as its potential uses in catalysis and as modifiable functional substrates.[24]

NU-1000 microcrystals were synthesized and activated according to the literature.[23] This led to size monodisperse NU-1000 microrods, although we also observed the occurrence of some cross-shaped particles, presumably due to NU-901 cocrystallization and subsequent NU-1000 growth on the NU-901 nodes (Figure S1).[20] To improve the dispersibility of the NU-1000 microcrystals in organic solvents, the NU-1000 was functionalized with trimethoxy(octadecyl)-silane (TMODS) to afford NU-1000$_{Si}$ (Figures S2 and S3). Infrared (IR) spectroscopy shows an IR absorption band at 3674 cm^{-1} corresponding to terminal −OH groups (from the zirconia clusters) on the NU-1000.[19] The functionalized NU-1000$_{Si}$ showed a decrease in the 3674 cm^{-1} band, consistent with expectations, as well as the occurrence of overlapping bands from 1130 to 930 cm^{-1}, attributed to Si−O−Si and Si−O−Zr bonds (Figure S4). Inductively coupled plasma-mass spectrometry (ICP-MS) of NU-1000$_{Si}$ showed the ratio of Zr:Si to be 1:1.39, or 8.3 Si per Zr_6 node. These findings can be explained by silyl ethers on the Zr_6 nodes further reacting with TMODS to form siloxy bridges. Powder X-ray diffraction (PXRD) also indicates that the NU-1000$_{Si}$ retains its crystalline framework structure after silanization (Figure S5).

Rectangular and square cross section capillary cells were prepared whereby opposite sides of the cells were coated with Au/Cr via e-beam deposition and connected to an AC source (Figure 2a). The capillaries were filled with NU-1000$_{Si}$/bromobenzene suspensions. Bromobenzene solvent was selected as its density (1.474 g·mL^{-1} at 25 °C) was relatively

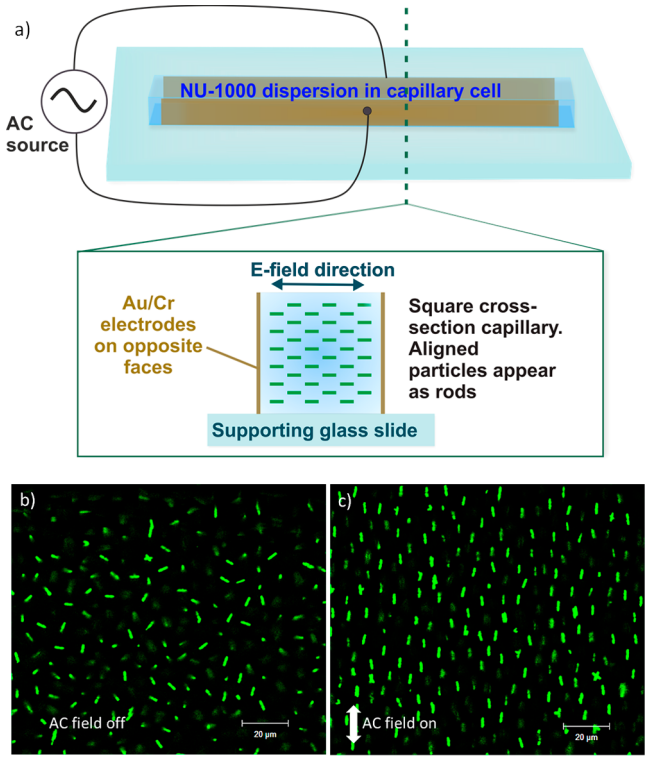

Figure 2. (a) Illustration of a capillary setup where the NU-1000$_{Si}$ suspension in the cell is exposed to an alternating E-field perpendicular to the viewing direction (top) and cross-sectional view of the glass capillary setup (bottom). Confocal microscope images of NU-1000$_{Si}$ suspensions in bromobenzene (b) without E-field, showing randomly oriented particles and (c) in the presence of 500 Hz, 37.5 V·mm^{-1} peak-to-peak E-field showing aligned particles.

closely matched with that of NU-1000$_{Si}$, giving stable suspensions across the time scale of weeks. Furthermore, bromobenzene with its low dielectric constant (ε = 5.19) and polarity possesses low electrolyte content, which affords relatively large inverse Debye screening lengths $1/\kappa$.[25] This facilitates large interparticle separations, which may allow for more rapid particle alignment. However, as the NU-1000$_{Si}$ scaffold is expected to have a high refractive index (different from the averaged refractive index of the MOF lattice and the pore-filling fluid) due to its zirconia nodes, it was not possible to find an index-matched solvent to minimize van der Waals interactions and light scattering. Nevertheless, by minimizing the thickness of the focal plane through decreasing the pinhole size, we were able to study the particle dispersions via confocal microscopy.

Conveniently, the pyrene-based ligand in NU-1000$_{Si}$ acts as a fluorophore, causing NU-1000$_{Si}$ to absorb 405 nm radiation and fluoresce at 470 nm, circumventing the need for additional dye functionalization for confocal microscopy. The NU-1000$_{Si}$ crystals are well separated by electrostatic repulsion, preventing their aggregation or gelation (Figure 2b) and show some order in their positional arrangement, despite their random orientation as well as thermal and Brownian motion (Figure S6). This is reminiscent of the colloidal plastic crystals or rotator phases described by van Blaaderen's group,[26] whereby interparticle electrostatic repulsions afford positional but not orientational order as the microrods rotate randomly around in their positions. However, the presence of the cross-shaped NU-1000$_{Si}$ particles appeared to disrupt the positional order

DOI: 10.1021/jacs.9b06320
J. Am. Chem. Soc. 2019, 141, 12989−12993

observed here. Upon exposure to an alternating E-field, however, the NU-1000$_{Si}$ microrods rapidly align along the E-field (Figure 2c). Under these conditions, we did not observe particle chaining of NU-1000$_{Si}$. Like in the case of electroresponsive SiO_2-based plastic crystals,[26] the observed interparticle repulsion prevents the particles from aggregating. Furthermore, as the tips of the NU-1000$_{Si}$ microrods are not perfectly flat, and the microrods surfaces were sterically stabilized by octadecylsiloxy groups, van der Waals based facet-to-facet attraction at the tips is expected to be relatively low.

To determine the electroresponse rate and extent, electrooptical measurements were carried out, using a polarized optical microscope and a photodetector (Thorlabs PDA100A Si Amplified Detector) to measure light transmission through the cell. NU-1000 crystallizes in the hexagonal space group *P6/mmm*[27,19] and is uniaxially birefringent. When viewed through crossed polarizers on an optical microscope, the particles appear blue against a dark background (Figure 3a). When the E-field is off, the NU-1000$_{Si}$ microrods are randomly oriented and undergo Brownian motion. Turning on the alternating E-field results in rapid, vertical microrod alignment (Figure 3a, particles appearing as blue dots), whereby the long axis of the microrods aligns with the light transmission direction and their effective light transmitting cross-sectional area decreases (Figure 3b,c). This is similar to previous observations of liquid crystalline niobate nanosheets where light propagation is minimized during particle alignment.[28] By plotting light transmission and E-field switching against time, we can determine the response rate and its extent. When the E-field is switched off, the particles relax slowly back into random orientations, and the light transmission returns to a maximum, as shown by the curved, unshaded sections of the graphs (Figure 3d).

The E-field alignment of NU-1000$_{Si}$ in bromobenzene is frequency dependent, with the most rapid alignment occurring at 500 Hz (0.1 s) (Figure S7). The E-field induces polarization of NU-1000$_{Si}$, and the particles align their axes of greatest polarizability along the field direction.[29] Particle polarization is induced through various mechanisms in an alternating E-field, with the mechanism dependent upon the field frequency and the particle material.[30,31] In this case, the low frequency suggests that the alignment process most likely takes place through Maxwell–Wagner–Sillars and O'Konski interfacial polarization.[32−35] In particular, we hypothesize that ions present within the NU-1000$_{Si}$ channels and in the electrical double layer on the external MOF particle–solvent interface undergo electromigration due to the imposed E-field.[36] These ions may result from the presence of adsorbed water and polar groups such as Zr–OH and Si–OH at the MOF–solvent interface[37,38] as well as from the sample preparation. Indeed, we found that the NU-1000$_{Si}$ particles possess negative ζ-potentials when dispersed in bromobenzene (Table S1). As the MOF channels run along the *c*-axis along the length of the microrods, induced dipoles arising from ion migration along the 1-D MOF channels cause E-field alignment of the NU-1000$_{Si}$ microrods. Further, since physisorption measurements of NU-1000$_{Si}$ showed it has a high specific surface area of 916 $m^2 \cdot g^{-1}$ and pore volume (Figures S8 and S9, Table S2), interfacial polarization effects are expected to be high.

We previously showed that magnetically aligned NU-1000/Sylgard 184 composites exhibited a fluoresence response which was dependent upon the angle of linearly polarized

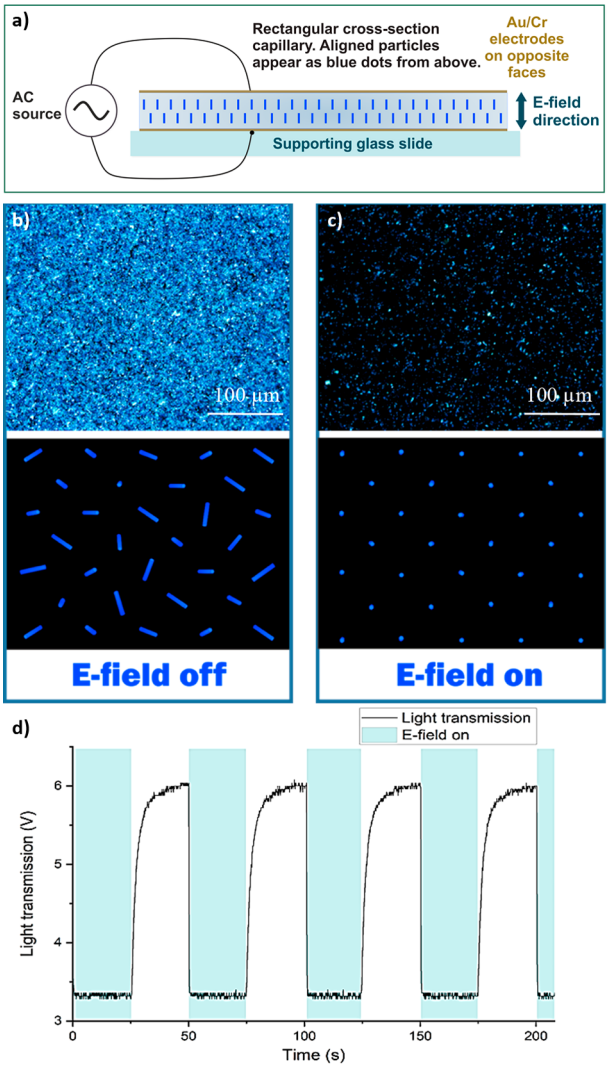

Figure 3. (a) Cross-sectional view of rectangular capillary used in electrooptical measurements. Electrical alignment of particles occurs vertically; (b) top and bottom, respectively: bright polarized optical microscopy (POM) image of 2 wt % NU-1000$_{Si}$ suspension in bromobenzene showing light transmission and an illustration depicting the random orientation of the crystals when E-field is off; (c) top and bottom, respectively: dark POM image of the same suspension showing decreased light transmission due to NU-1000$_{Si}$ alignment along the alternating E-field, perpendicular to the plane of the paper and illustration depicting the particle alignment. (d) Electrooptical response of the suspension–light transmission under alternating E-field (100 $V \cdot mm^{-1}$ peak-to-peak, 500 Hz).

excitation.[22] This dependence arises from the lattice anisotropy of NU-1000, as the pyrene-based TBAPy ligands are oriented along the *c*-axis (Figure 1) and hence absorb linearly polarized excitation anisotropically. Drawing upon this, we carried out fluorescence response studies on NU-1000$_{Si}$ suspensions. The samples were irradiated at normal incidence to the sample plane with 405 nm linearly polarized excitation, and their photoluminescence anisotropy determined. A half-wave plate was used to adjust the polarization angle of the incident light, and measurements were taken at 10° intervals (Figure 4a). The azimuthal plot in Figure 4 shows the integrated fluorescence intensity, normalized to its maximum value. When the NU-1000$_{Si}$ particles are electrically aligned, the photoluminescence response is significantly dependent upon the polarization angle

DOI: 10.1021/jacs.9b06320
J. Am. Chem. Soc. 2019, 141, 12989−12993

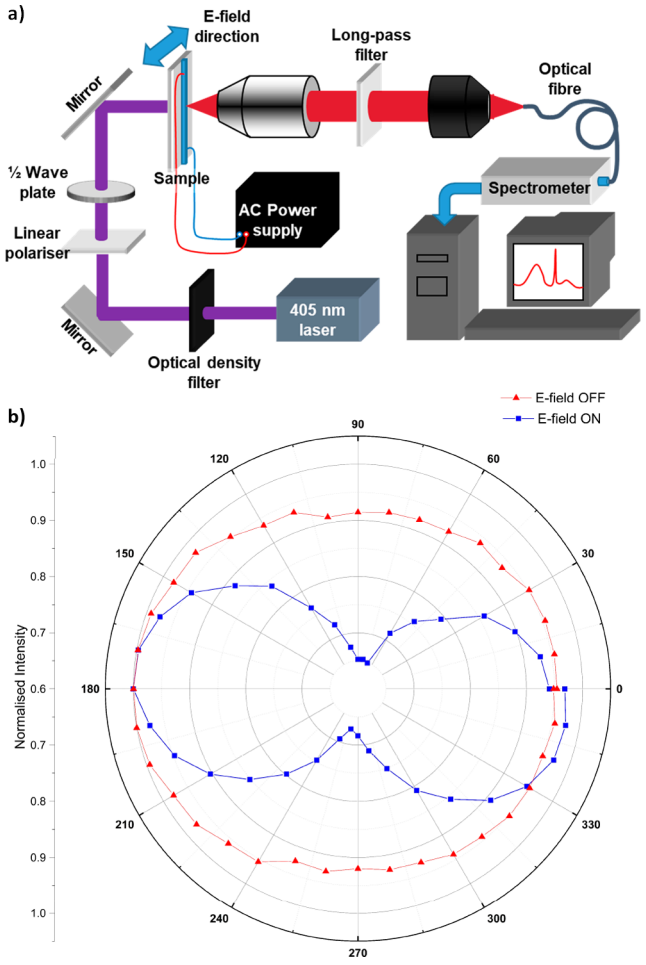

Figure 4. (a) Fluorescence response study setup. (b) Azimuthal plot of fluorescence intensity response of NU-1000$_{Si}$ particles in bromobenzene in a 500 Hz 100 V·mm^{-1} peak-to-peak E-field when the field is ON (blue) and OFF (red). E-field orientation is at 0°.

of the excitation relative to the E-field and MOF alignment direction. The highest fluorescence intensity is observed when the polarization angle of incident light is 0° to the E-field direction whereas the fluorescence minima occurs when the angle is 90°, in accordance to expectations.

In conclusion, we have demonstrated dynamic NU-1000$_{Si}$ alignment through E-field switching, and shown reversible electrooptical responses as well as orientationally dependent fluorescence response of the NU-1000$_{Si}$ dispersions. Such an approach is expected to be applicable to a wide variety of MOFs, as their high surface areas should allow for interfacial polarization and E-field alignment. As such, this work is expected to open up possibilities for the development of switchable MOF assemblies and devices. Future work will focus on the detailed investigation of the parameters required for applying E-field alignment to other MOFs, such as the effect of MOF network topology and pore structure, ion concentration, particle surface functionalities and solvent selection on their E-field alignment.

■ ASSOCIATED CONTENT

Supporting Information

The Supporting Information is available free of charge on the ACS Publications website at DOI: 10.1021/jacs.9b06320.

Experimental details and characterization results (PDF)

Video showing electrooptical switching of NU-1000$_{Si}$ in bromobenzene (100 V·mm^{-1} peak-to-peak, 500 Hz) viewed through crossed polarizers on an optical microscope (MP4)

Video showing E-field induced alignment of NU-1000$_{Si}$ in bromobenzene as viewed through a confocal microscope where individual NU-1000$_{Si}$ rods can be seen (100 V·mm^{-1} peak-to-peak, 1 kHz) (MP4)

■ AUTHOR INFORMATION

Corresponding Authors

*j.chin@hull.ac.uk

*michael.reithofer@univie.ac.at

ORCID

Neil T. Kemp: 0000-0002-1906-4608

Ali M. Adawi: 0000-0001-6850-5679

Freddy Kleitz: 0000-0001-6769-4180

Arnout Imhof: 0000-0002-7445-1360

Michael R. Reithofer: 0000-0002-6328-1896

Jia Min Chin: 0000-0002-0540-1597

Author Contributions

¶These authors contributed equally.

Notes

The authors declare no competing financial interest.

■ ACKNOWLEDGMENTS

The authors thank the University of Vienna and the University of Hull for providing the financial support to carry out this work. A.J.Y. thanks the University of Hull for the provision of his University scholarship.

■ REFERENCES

(1) Zhou, H.-C.; Long, J. R.; Yaghi, O. M. Introduction to Metal–Organic Frameworks. *Chem. Rev.* **2012**, *112*, 673–674.

(2) Furukawa, H.; Cordova, K. E.; O'Keeffe, M.; Yaghi, O. M. The Chemistry and Applications of Metal-Organic Frameworks. *Science* **2013**, *341*, 1230444.

(3) Wang, H.; Zhu, Q.-L.; Zou, R.; Xu, Q. Metal-Organic Frameworks for Energy Applications. *Chem.* **2017**, *2*, 52–80.

(4) Biemmi, E.; Scherb, C.; Bein, T. Oriented Growth of the Metal Organic Framework Cu3(BTC)2(H2O)3·xH2O Tunable with Functionalized Self-Assembled Monolayers. *J. Am. Chem. Soc.* **2007**, *129*, 8054–8055.

(5) Tan, T. T. Y.; Reithofer, M. R.; Chen, E. Y.; Menon, A. G.; Hor, T. S. A.; Xu, J.; Chin, J. M. Tuning Omniphobicity via Morphological Control of Metal–Organic Framework Functionalized Surfaces. *J. Am. Chem. Soc.* **2013**, *135*, 16272–16275.

(6) Falcaro, P.; Okada, K.; Hara, T.; Ikigaki, K.; Tokudome, Y.; Thornton, A. W.; Hill, A. J.; Williams, T.; Doonan, C.; Takahashi, M. Centimetre-scale micropore alignment in oriented polycrystalline metal–organic framework films via heteroepitaxial growth. *Nat. Mater.* **2017**, *16*, 342.

(7) Tarzia, A.; Takahashi, M.; Falcaro, P.; Thornton, A. W.; Doonan, C. J.; Huang, D. M. High-Throughput Screening of Metal–Organic Frameworks for Macroscale Heteroepitaxial Alignment. *ACS Appl. Mater. Interfaces* **2018**, *10*, 40938–40950.

(8) Stassen, I.; Burtch, N.; Talin, A.; Falcaro, P.; Allendorf, M.; Ameloot, R. An updated roadmap for the integration of metal–organic frameworks with electronic devices and chemical sensors. *Chem. Soc. Rev.* **2017**, *46*, 3185–3241.

(9) Zhou, S.; Wei, Y.; Li, L.; Duan, Y.; Hou, Q.; Zhang, L.; Ding, L.-X.; Xue, J.; Wang, H.; Caro, J. Paralyzed membrane: Current-driven

synthesis of a metal-organic framework with sharpened propene/propane separation. *Science Advances* **2018**, *4*, eaau1393.
(10) Winston, E. B.; Lowell, P. J.; Vacek, J.; Chocholoušová, J.; Michl, J.; Price, J. C. Dipolar molecular rotors in the metal−organic framework crystal IRMOF-2. *Phys. Chem. Chem. Phys.* **2008**, *10*, 5188−5191.
(11) Namsani, S.; Yazaydin, A. O. Electric field induced rotation of halogenated organic linkers in isoreticular metal−organic frameworks for nanofluidic applications. *Mol. Syst. Des. Eng.* **2018**, *3*, 951−958.
(12) Knebel, A.; Geppert, B.; Volgmann, K.; Kolokolov, D. I.; Stepanov, A. G.; Twiefel, J.; Heitjans, P.; Volkmer, D.; Caro, J. Defibrillation of soft porous metal-organic frameworks with electric fields. *Science* **2017**, *358*, 347−351.
(13) Ghoufi, A.; Benhamed, K.; Boukli-Hacene, L.; Maurin, G. Electrically Induced Breathing of the MIL-53(Cr) Metal−Organic Framework. *ACS Cent. Sci.* **2017**, *3*, 394−398.
(14) Schmid, R. An Electric Field Induced Breath for Metal−Organic Frameworks. *ACS Cent. Sci.* **2017**, *3*, 369−371.
(15) Kolesnikov, A. L.; Budkov, Y. A.; Möllmer, J.; Kiselev, M. G.; Gläser, R. Metal−Organic Framework Breathing in the Electric Field: A Theoretical Study. *J. Phys. Chem. C* **2019**, *123*, 10333−10338.
(16) Hod, I.; Bury, W.; Karlin, D. M.; Deria, P.; Kung, C.-W.; Katz, M. J.; So, M.; Klahr, B.; Jin, D.; Chung, Y.-W.; Odom, T. W.; Farha, O. K.; Hupp, J. T. Directed Growth of Electroactive Metal-Organic Framework Thin Films Using Electrophoretic Deposition. *Adv. Mater.* **2014**, *26*, 6295−6300.
(17) Yanai, N.; Sindoro, M.; Yan, J.; Granick, S. Electric Field-Induced Assembly of Monodisperse Polyhedral Metal−Organic Framework Crystals. *J. Am. Chem. Soc.* **2013**, *135*, 34−37.
(18) Liu, Y. D.; Kim, J.; Ahn, W.-S.; Choi, H. J. Novel electrorheological properties of a metal−organic framework $Cu_3(BTC)_2$. *Chem. Commun.* **2012**, *48*, 5635−5637.
(19) Deria, P.; Mondloch, J. E.; Tylianakis, E.; Ghosh, P.; Bury, W.; Snurr, R. Q.; Hupp, J. T.; Farha, O. K. Perfluoroalkane Functionalization of NU-1000 via Solvent-Assisted Ligand Incorporation: Synthesis and CO_2 Adsorption Studies. *J. Am. Chem. Soc.* **2013**, *135*, 16801−16804.
(20) Islamoglu, T.; Otake, K.-i.; Li, P.; Buru, C. T.; Peters, A. W.; Akpinar, I.; Garibay, S. J.; Farha, O. K. Revisiting the structural homogeneity of NU-1000, a Zr-based metal−organic framework. *CrystEngComm* **2018**, *20*, 5913−5918.
(21) Vargas, L. E.; Snurr, R. Q. Heterogeneous Diffusion of Alkanes in the Hierarchical Metal−Organic Framework NU-1000. *Langmuir* **2015**, *31*, 10056−10065.
(22) Cheng, F.; Marshall, E. S.; Young, A. J.; Robinson, P. J.; Bouillard, J. S. G.; Adawi, A. M.; Vermeulen, N. A.; Farha, O. K.; Reithofer, M. R.; Chin, J. M. Magnetic Control of MOF Crystal Orientation and Alignment. *Chem. - Eur. J.* **2017**, *23*, 15578−15582.
(23) Wang, T. C.; Vermeulen, N. A.; Kim, I. S.; Martinson, A. B. F.; Stoddart, J. F.; Hupp, J. T.; Farha, O. K. Scalable synthesis and post-modification of a mesoporous metal-organic framework called NU-1000. *Nat. Protoc.* **2016**, *11*, 149.
(24) Ahn, S.; Nauert, S. L.; Buru, C. T.; Rimoldi, M.; Choi, H.; Schweitzer, N. M.; Hupp, J. T.; Farha, O. K.; Notestein, J. M. Pushing the Limits on Metal−Organic Frameworks as a Catalyst Support: NU-1000 Supported Tungsten Catalysts for *o*-Xylene Isomerization and Disproportionation. *J. Am. Chem. Soc.* **2018**, *140*, 8535−8543.
(25) Yethiraj, A.; van Blaaderen, A. A colloidal model system with an interaction tunable from hard sphere to soft and dipolar. *Nature* **2003**, *421*, 513.
(26) Liu, B.; Besseling, T. H.; Hermes, M.; Demirörs, A. F.; Imhof, A.; van Blaaderen, A. Switching plastic crystals of colloidal rods with electric fields. *Nat. Commun.* **2014**, *5*, 3092.
(27) Mondloch, J. E.; Bury, W.; Fairen-Jimenez, D.; Kwon, S.; DeMarco, E. J.; Weston, M. H.; Sarjeant, A. A.; Nguyen, S. T.; Stair, P. C.; Snurr, R. Q.; Farha, O. K.; Hupp, J. T. Vapor-Phase Metalation by Atomic Layer Deposition in a Metal−Organic Framework. *J. Am. Chem. Soc.* **2013**, *135*, 10294−10297.
(28) Nakato, T.; Nakamura, K.; Shimada, Y.; Shido, Y.; Houryu, T.; Iimura, Y.; Miyata, H. Electrooptic Response of Colloidal Liquid Crystals of Inorganic Oxide Nanosheets Prepared by Exfoliation of a Layered Niobate. *J. Phys. Chem. C* **2011**, *115*, 8934−8939.
(29) Koerner, H.; Jacobs, J. D.; Tomlin, D. W.; Busbee, J. D.; Vaia, R. A. Tuning Polymer Nanocomposite Morphology: AC Electric Field Manipulation of Epoxy−Montmorillonite (Clay) Suspensions. *Adv. Mater.* **2004**, *16*, 297−302.
(30) Tabbagh, A.; Cosenza, P.; Ghorbani, A.; Guérin, R.; Florsch, N. Modelling of Maxwell−Wagner induced polarisation amplitude for clayey materials. *J. Appl. Geophys.* **2009**, *67*, 109−113.
(31) Filisko, F. E.; Radzilowski, L. H. An intrinsic mechanism for the activity of alumino-silicate based electrorheological materials. *J. Rheol.* **1990**, *34*, 539−552.
(32) Kremer, F.; Schönhals, A. *Broadband dielectric spectroscopy*; Springer: New York, 2003.
(33) Maxwell, J. C. *A treatise on electricity and magnetism*; Clarendon Press: Oxford, 1873; Vol. *1*.
(34) Wagner, K. W. Erklärung der dielektrischen nachwirkungsvorgänge auf grund maxwellscher vorstellungen. *Arch. Elektrotech.* **1914**, *2*, 371−387.
(35) Sillars, R. The properties of a dielectric containing semiconducting particles of various shapes. *J. Inst. Electr. Eng.* **1937**, *80*, 378−394.
(36) Shilov, V. N.; Delgado, A. V.; González-Caballero, F.; Horno, J.; López-García, J. J.; Grosse, C. Polarization of the Electrical Double Layer. Time Evolution after Application of an Electric Field. *J. Colloid Interface Sci.* **2000**, *232*, 141−148.
(37) Goodwin, J. W.; McDonald, F.; Reynolds, P. A. The effect of trace water on non-aqueous silica dispersions. *Colloids Surf.* **1988**, *33*, 1−9.
(38) Hao, T.; Kawai, A.; Ikazaki, F. Mechanism of the Electrorheological Effect: Evidence from the Conductive, Dielectric, and Surface Characteristics of Water-Free Electrorheological Fluids. *Langmuir* **1998**, *14*, 1256−1262.

DOI: 10.1021/jacs.9b06320
J. Am. Chem. Soc. 2019, 141, 12989−12993